Applied Catalysis B: Environmental 258 (2019) 117995

Contents lists available at ScienceDirect

Applied Catalysis B: Environmental

journal homepage: www.elsevier.com/locate/apcatb

Insight into the superior activity of bridging sulfur-rich amorphous molybdenum sulfide for electrochemical hydrogen evolution reaction

Cheol-Ho Lee[a,b,1], Sungho Lee[a,c,1], Gil-Seong Kang[a,b], Youn-Ki Lee[a], Gwan Gyu Park[d], Doh C. Lee[b], Han-Ik Joh[d,*]

[a] Carbon Composite Materials Research Center, Institute of Advanced Composite Materials, Korea Institute of Science and Technology (KIST), 92 chudong-ro, Bongdong-eup, Wanju, Jeollabukdo 55324, Republic of Korea
[b] Department of Chemical and Biomolecular Engineering (BK21 + Program), KAIST Institute for the Nanocentury, Korea Advanced Institute of Science and Technology (KAIST), Daejeon 34141, Republic of Korea
[c] Department of Nano Material Engineering, Korea University of Science and Technology, 217 Gajeong-ro, Yuseong-gu, Daejeon 34113, Republic of Korea
[d] Department of Energy Engineering, Konkuk University, 120 Neungdong-ro, Gwangjin-gu, Seoul 05029, Republic of Korea

ARTICLE INFO

Keywords:
Bridging sulfur
Amorphous molybdenum sulfide
Electrocatalyst
Hydrogen evolution reaction

ABSTRACT

Hydrogen evolution reaction (HER) activity of the molybdenum sulfide-based electrocatalysts originates from diverse types of active sulfur (S) sites, different S configurations, the ratio of molybdenum to S, and the crystallinity. The bridging S_2^{2-} has been considered as the major active site for HER. However, to realize more efficient electrocatalysts, newer architectures based on molybdenum sulfide are required to allow more active S sites beyond the endemic structural limits. Hence, the facile aging approach is used to maximize the bridging S_2^{2-} in amorphous molybdenum sulfide by adding $(NH_4)_2S_x$, leading to the highest proportion of bridging S_2^{2-} (up to 67%). Additionally, the effect of S configuration on HER activity in molybdenum sulfide is systematically studied by controlling of the amount of bridging S_2^{2-}. The bridging S-rich electrocatalysts exhibits an excellent HER activity with low onset potential of −96 mV and Tafel slope of 46 mV dec^{-1}, and stability for 1000 cycles.

1. Introduction

The energy and environmental crisis facing the world have required clean, sustainable, and load-balanceable energy paradigm beyond the existing fossil fuel-based system. Molecular hydrogen (H_2) produced by water splitting have been expected to realize the global demand for the energy. To popularize this process, numerous studies have been carried out to develop efficient and cheap electrocatalysts for the hydrogen evolution reaction (HER) [1–4]. Electrocatalysts based on molybdenum sulfides are some of the most promising materials for HER due to their low Gibb's free energy (~0.08 eV) for hydrogen adsorption [5]. Among the various kinds of molybdenum sulfides, crystalline molybdenum disulfide (c-MoS_2) based electrocatalysts have been extensively investigated for decades [6–17]. However, c-MoS_2 exhibits less HER activity than platinum, which is commercially available one with the highest activity in acidic solutions. This results from a relatively narrow electrochemically active area in c-MoS_2. It is known that only the edge of the c-MoS_2 was electrochemically active, while the basal plane was electrochemically inert [5].

Innovative designs for molybdenum sulfides have been considered to improve this critical issue [18–21]. Thiomolybdate clusters, $[Mo_3S_{13}]^{2-}$ on a graphitic paper or carbon nanotubes, are known to have intrinsically exposed sulfur atoms throughout the surface of the clusters unlike c-MoS_2, leading to the best activity among molybdenum sulfide based electrocatalysts [22,23]. It was experimentally proved by the selective removal of sulfur (S) that the major active sites in molybdenum sulfides were bridging S sites in the clusters, while the terminal S sites were electrochemically inert [24,25]. From a structural viewpoint, S atoms are preferentially bonded to molybdenum as terminal S rather than bridging S configuration, since the terminal S with saturated S^{2-} state is more stable than the bridging S with unsaturated S_2^{2-} state. Therefore, it is necessary that bridging S-rich molybdenum sulfides should be newly designed to enhance HER activity up to the level of platinum.

Recent studies reported a simple strategy to synthesize molybdenum sulfides with higher S/Mo ratio, in order to increase the bridging S_2^{2-} configuration in molybdenum sulfides [8]. Ye et al. synthesized MoS_x/CNT nanospheres (x = 3.8) by ultrasonic spray and pyrolysis at 300 °C

* Corresponding author.
E-mail address: hijoh@konkuk.ac.kr (H.-I. Joh).
[1] These authors (C.-H.Lee and S.Lee) contributed equally to this study.

https://doi.org/10.1016/j.apcatb.2019.117995
Received 12 April 2019; Received in revised form 19 July 2019; Accepted 22 July 2019
Available online 24 July 2019
0926-3373/

[26]. Even though the molybdenum sulfides were optimally synthesized to increase the bridging S content, HER activity (overpotential of 168 mV at 10 mA cm^{-2} and Tafel slope of 36 mV dec^{-1}) was relatively lower than other structurally-modified molybdenum sulfides in other open literatures. Similarly, Wang et al. also synthesized MoS_x (x = 5) on polypyrrole by electrodeposition, which can realize the facile control of ratio between Mo and S, leading to an increase in bridging S_2^{2-} and subsequent HER activity [27]. However, the effect of Mo/S ratio on various sulfur configurations and the mechanism of forming higher content of bridging S in the molybdenum sulfide-based catalysts was not discussed in detail.

In this study, we reported a facile approach to maximize the amount of bridging S_2^{2-} configuration, which is the most active site for HER in amorphous molybdenum sulfides (a-MoS_x), by the addition of ammonium polysulfide. There is a suitable "aging time" for the reaction of molybdenum sulfide with ammonium polysulfide that leads to the highest proportion of bridging S_2^{2-} (up to 67%) in amorphous molybdenum sulfide. To verify the formation mechanism of maximum bridging S sites, various kinds of ions generated during the reaction were selectively removed by precipitimetry of the oppositely charged ions. Additionally, the interrelationship between ratios of bridging S_2^{2-} in the entire S configuration, and HER activity of the catalysts was demonstrated by modulating the electrochemically active sites. It is expected that an insight into the new molybdenum sulfide-based architectures would allow us to realize new H_2 based paradigms.

2. Experimental

2.1. Synthesis of molybdenum sulfide

Ammonium tetrathiomolybdate (0.4 g) ($(NH_4)_2MoS_4$, Sigma-Aldrich, USA) and 18–21% ammonium polysulfide (0–7 mL) ($(NH_4)_2S_x$, Alfa Aesar, USA) solution were dissolved in distilled water (100 mL) by bath-sonication and stirring, followed by refrigeration of the mixture at 2 °C for 12 h. Subsequently, hydrochloric acid (HCl) (10 mL) was slowly added to the mixture, accompanied by constant stirring for 30 min. The resulting powder was filtered using a vacuum filter. To remove the residual S, the filtered powder was dissolved and washed in toluene at 80 °C for 24 h by stirring. Finally, the product was obtained by filtration and subsequent washing with toluene, dimethylformamide, and distilled water, followed by freeze drying.

2.2. Structural analysis of $(NH_4)_2MoS_4$ and $(NH_4)_2S_x$ mixtures

The structural properties of the $(NH_4)2MoS_4$ and $(NH_4)_2S_x$ mixtures were investigated using Raman (Renishaw, UK) and UV–vis spectrometry (V-670, Jasco, Japan). $(NH_4)_2MoS_4$ and $(NH_4)_2S_x$ mixture (0.2 mL) was diluted with distilled water (10 mL). To obtain crystalline molybdenum sulfide anions, tetraethyl ammonium chloride or tetraphenylphosphonium chloride (1 g) (Sigma-Aldrich, USA) was added to the mixture and kept for 12 h. Finally, the solution was filtered, and the obtained powder was washed using distilled water.

2.3. Characterizations

The structures of crystalline molybdenum sulfide anions and amorphous MoS_x were analyzed using X-ray diffraction (XRD, Smartlab 3, Rigaku, Japan) at a scan rate of 2° min^{-1} from 5 to 60°. Chemical properties were analyzed using an X-ray photoelectron spectroscope (XPS, Multilab 2000, Thermo Fisher, USA) equipped with a monochromatic Al Kα (hv = 1000 eV) X-ray source. The morphologies were investigated using a scanning electron microscope (SEM, Nova Nano SEM 450, FEI, USA) and a transmission electron microscope (TEM, Technai G2 F20, Thermo Fisher Scientific, USA).

2.4. Electrochemical analyses

To fabricate an electrode solution, each sample (7.5 mg), along with carbon nanotube mixture (7.5 mg), was dispersed in dimethylformamide (1 mL) using a bath-sonicator. Subsequently, Nafion solution (100 μL) was added to the solution as a binder. The electrode solution (8 μL) was coated on 0.196 cm^2 of glassy carbon electrode and dried at 60 °C. Average weight of MoS_x on the electrode was measured using a digital analytical balance (GH-252, A&D Company, Limited, Japan). First, 80 μL of the solution was dropped on filter paper and dried at 60 °C oven for 1 h. The weight of filter paper before and after solution loading of 80 μL was measured to obtain the weight difference. The weight of MoS_x (dried solution loading, 80 μL) is approximately 117.6 μg. By the following equation, the weight of electrode per an unit area of the working electrode was obtained.

$$\text{weight of } MoS_x \text{ on the electrode } (\mu g\, cm^{-2}) = (\text{weight of } MoS_x \text{ on filter paper } \mu g) * (8\,\mu L/80\,\mu L)/(0.196\, cm^2) \quad (1)$$

where, the calculated average weight of MoS_x on an electrode was approximately 60 μg cm^{-2}.

The electrochemical cyclic voltammetry, linear sweep, and impedance spectroscopy were measured using an electrochemical analysis device (AUT302M FRA2, Metrohm Autolab, Netherlands) in N_2 bubbled 0.5 M H_2SO_4 electrolyte. Pt wire and Ag/AgCl electrode were used as counter and reference electrodes, respectively. To calculate the electrochemical surface area, cyclic voltammetry was carried out in the potential range from −0.1 to 0.1 V. Electrochemical HER activity was measured by linear sweep voltammetry from 0.1 to −0.3 V (vs RH) at a scan rate of 5 mV s^{-1} at 1600 rpm. Electrochemical impedance spectroscopy (EIS) was recorded at 0.1 V from 10^6 to 0.02 Hz with AC voltage of 5 mV.

2.5. Calculation of turnover frequency (TOF)

To calculate the TOF, the following equation was used:

$$\text{TOF} = \frac{\textit{Number of total hydrogen} / \text{cm}^2}{\textit{Number of active sites} / \text{cm}^2} \quad (2)$$

The total number of hydrogen atoms was calculated using current density at 200 mV.

The number of active sites on an electrode was calculated by the following formula:

$$\text{Mo atoms} / \text{cm}^2 = \frac{60\,\mu g/\text{cm}^2}{\textit{molar weight of } MoS_x\ (g/mol)} \times (6.02 \times 10^{23} Mo \frac{atoms}{\text{mol}}) \quad (3)$$

3. Results and discussion

3.1. Synthesis of a-MoS_x and S_{br}-MoS_x

Various kinds of molybdenum sulfides, such as MoS_2, $[Mo_3S_{13}]^{2-}$ cluster, and Mo_2S_{12} have their own characteristic structures based on molecular thermal dynamics, which result in chemically stable and crystalline structures. Considering a-MoS_3, there are various kinds of Mo-S bonding, different chemical states of Mo and S atoms, and even differing morphologies. Therefore, we believed that a-MoS_3 can be taken as the suitable starting material to precisely control S configuration. Traditionally, a-MoS_3 was simply prepared by the reaction of ammonium tetrathiomolybdate ($(NH_4)_2MoS_4$) with hydrochloric acid (HCl) [28]. To enrich the bridging S configuration in a-MoS_x, we used a facile aging approach to maximize the bridging S_2^{2-} in a-MoS_3. The configuration change of S in bridging S enriched a-MoS_x (S_{br}-MoS_x) with a various addition of ammonium polysulfide was investigated

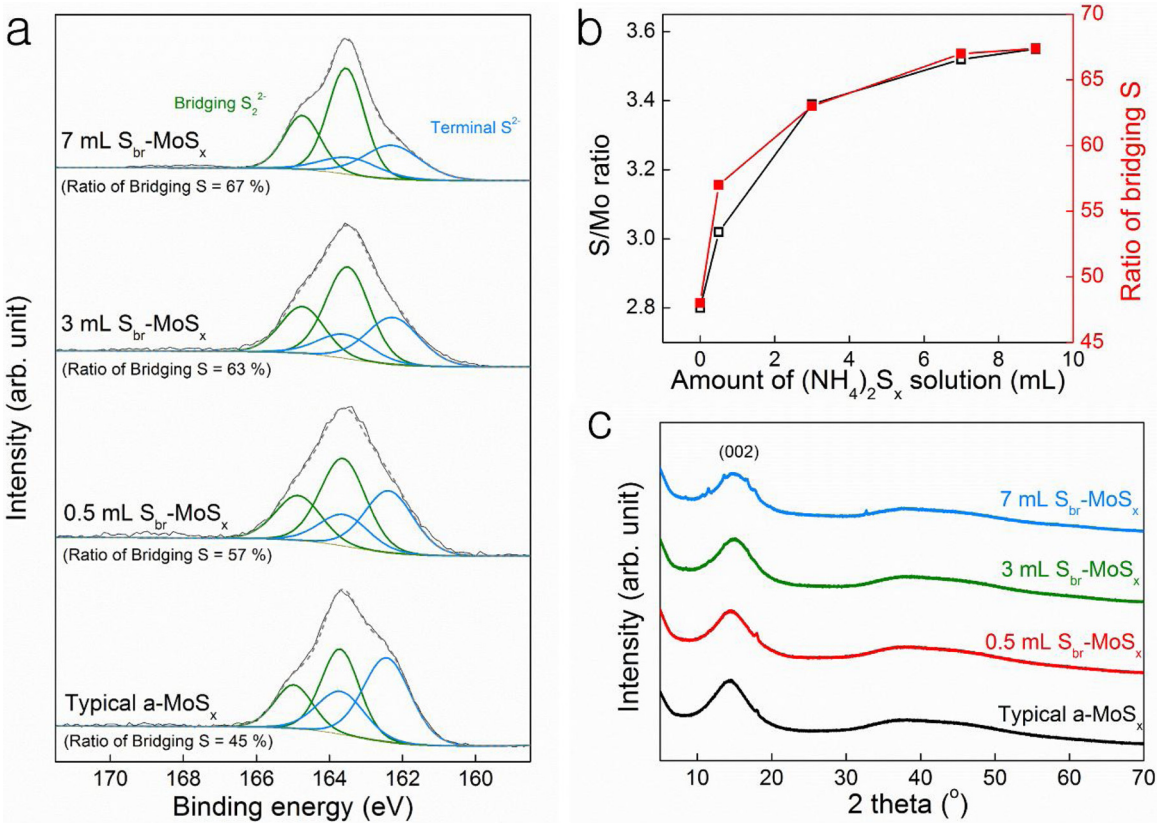

Fig. 1. (a) Deconvoluted XPS S2p spectra of typical a-MoS_x and S_{br}-MoS_x, (b) S/Mo ratio and atomic percent of bridging S, and (c) XRD diffractogram of typical a-MoS_x and S_{br}-MoS_x with various ammonium polysulfide contents (0.5–7 mL).

using X-ray photoelectron spectroscopy (XPS), as shown in Fig. 1a. The S2p spectra of molybdenum sulfides were composed of terminal S_2^{2-} doublet at 162.4 and 163.8 eV, and bridging S^{2-} doublet at 163.7 and 165.0 eV, respectively. As the added amount of ammonium polysulfide increased from 0.5 to 7 mL, an atomic percent of bridging S_2^{2-} to the entire S content in the S_{br}-MoS_x increased significantly from 57% to 67%. Interestingly, the ratio of bridging S configuration had dramatically increased even though a small amount of ammonium polysulfide (0.5 mL) was added in the pre-reaction. Comparing the S_{br}-MoS_x (67% of bridging S configuration) prepared with 7 mL solution of ammonium polysulfide to a typical a-MoS_x (45% of bridging S configuration), the difference in the atomic percent is 22% and 49% as absolute and relative values, respectively. Similar structural changes could be observed in Mo3d as shown in Fig. S1. The Mo3d spectra of molybdenum sulfides for the two electronic states of molybdenum show a major doublet at 228.9 and 232.0 eV, and a minor doublet at 230.5 and 233.6 eV for Mo^{4+} and Mo^{5+} oxidation state, respectively [29]. The proportion of Mo^{5+} in Mo 3d decreased with increasing ammonium polysulfide content, indicating the reduction of molybdenum atoms. The S2s spectra, which could be attributed to S_2^{2-} and S^{2-} state at 227.2 and 225.6 eV, respectively [27], were also observed in the range of lower electron binding energy from 224 to 228 eV. By deconvoluting the S2s spectra, the atomic percent of bridging S_2^{2-} in the S_{br}-MoS_x was quantitatively confirmed to be 45% and 67% in a-MoS_x and S_{br}-MoS_x (prepared by adding 7 mL ammonium polysulfide), respectively, even though there is a minor deviation of 2% in the case of S_{br}-MoS_x. Note that catalysts containing y% of bridging S_2^{2-} in original amorphous and bridging S-rich MoS_x are denoted as y% a-MoS_x and y% S_{br}-MoS_x, respectively. The S/Mo ratios of 57%, 63%, and 67% S_{br}-MoS_x were approximately 3.0, 3.4, and 3.5, respectively, while the S/Mo ratio of 45% a-MoS_x was only 2.8 (Fig. 1b and Table S1.). It was indicated that the pre-reaction of ammonium tetrathiomolybdate with ammonium polysulfide could not only induce the formation of bridging S configuration, but also increase the entire content of S atoms in the S_{br}-MoS_x. However, we observed a saturation point in the bridging S_2^{2-} content at 7 ml of $(NH_4)_2S_x$, and subsequently there was no significant increase in the bridging S_2^{2-} content, even when the volume of $(NH_4)_2S_x$ was increased up to 9 mL, as shown in Fig. 1b. The morphologies of 45% a-MoS_x and 67% S_{br}-MoS_x were investigated using a scanning electron microscope (SEM) and a high resolution-transmission electron microscope (HR-TEM) as shown in Fig. S2 and 3, respectively. All samples showed irregularly entangled shapes or aggregated particles in terms of macroscopic shape. Even though small and short fringes in both samples could be observed by HR-TEM, the amorphous structures of 45% a-MoS_x and 67% S_{br}-MoS_x were confirmed by X-ray diffractogram. Only a broad (002) peak at 14.4°, which is related to the typical amorphous MoS_x[18], was observed as shown in Fig. 1c. Therefore, we believed that both 45% a-MoS_x and 67% S_{br}-MoS_x have similar morphological and structural properties even though the S/Mo ratio and atomic contents of bridging S configuration increased via pre-reaction with ammonium polysulfide.

3.2. Electrochemical characteristics for HER

To increase the electrical conductivity of MoS_x based electrocatalysts, 45% a-MoS_x, and 57%, 63%, and 67% S_{br}-MoS_x were deposited on the oxidized carbon nanotubes by mechanical mixing before electrochemical HER evaluation [24]. Fig. 2a showed IR compensated electrochemical linear sweeps of all samples in 0.5 M H_2SO_4 solution. The overpotential at 10 mA cm^{-2} and Tafel slope of 45% a-MoS_x were approximately −0.143 V and 58 mV dec^{-1}, respectively (Fig. 2b). Interestingly, overpotential values (−0.139, −0.129, and −0.118 V) and Tafel slopes (49, 47, and 46 mV dec^{-1}) for 57%, 63%, and 67% S_{br}-MoS_x, respectively, were gradually enhanced with an increase in the

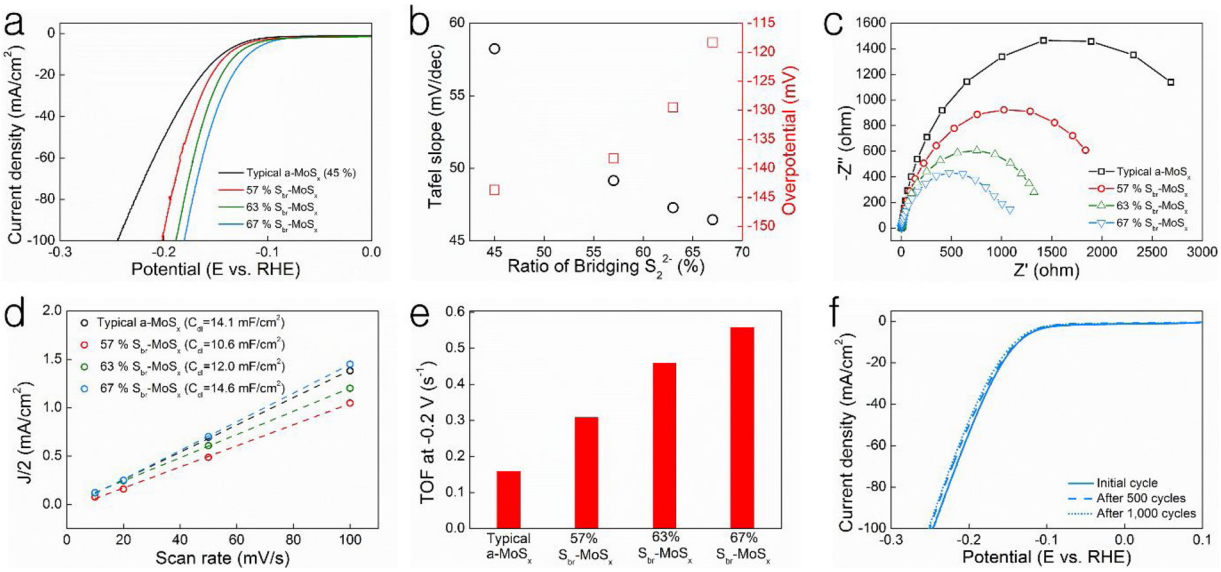

Fig. 2. (a) Linear sweep voltammetry, (b) tafel slope and overpotential at 10 mA cm^{-2}, (c) electrochemical impedance spectra, (d) electrochemical capacitance calculated from CV, (e) TOF value of typical a-MoS_x and S_{br}-MoS_x with bridging S contents in the range from 51 to 67%, and (f) HER activity of 67% S_{br}-MoS_x before and after cycling test.

bridging S configuration, and 67% S_{br}-MoS_x finally showed the highest electrochemical HER activity. The effect of the bridging S configuration on electrochemical properties of the catalysts was investigated as shown in Fig. 2c–e. The charge transport resistance of the S_{br}-MoS_x dramatically decreased with an increase in the amount of bridging S configuration. While comparing 57% S_{br}-MoS_x to 45% a-MoS_x, it is worthy to note that such a slight increase by 12% in the bridging S configuration of the catalysts significantly resulted in increasing the charge transport. The electrochemical surface area of the samples was calculated using cyclic voltammogram as a function of scan rate in the range from –0.10 to 0.10 V (Fig. S4). At a low scan rate, there are no significant differences between the samples, while a small deviation was observed at moderate and high scan rates (Fig. 2d and Fig. S4). In this study, HER properties of all samples were analyzed at 5 mV s^{-1}. Therefore, we believed that the effect of electrochemical surface area on the activity could be negligible. Turnover frequency (TOF), as an intrinsic property of a catalyst, was investigated using the procedures described in Experimental Section. TOF values were significantly enhanced from 0.15 s^{-1} for 45% a-MoS_x to 0.31, 0.46, and 0.56 s^{-1} for 57%, 63%, and 67% S_{br}-MoS_x, respectively, even though S_{br}-MoS_x catalysts possessed slightly low active sites calculated on the basis of the number of Mo atoms (1.88×10^{17}, 1.76×10^{17}, and 1.73×10^{17} Mo atoms for 57%, 63%, and 67% S_{br}-MoS_x, respectively) compared to 45% a-MoS_x (1.94×10^{17} Mo atoms) as shown in Fig. 2e. Considering TOF values and active sites calculated on the basis of the number of bridging S configurations, it was evident that both these parameters for 67% S_{br}-MoS_x were superior to those for 45% a-MoS_x (Table S2). Therefore, it may be concluded that an increase in the bridging S configuration in the MoS_x affects a large number of electrochemical adsorption sites, lowers the thermal dynamic energy of adsorbates and desorbates, and enhances charge transport due to electronic modulation, leading to superior HER activity as compared to other molybdenum sulfide-based catalysts in the open literature. The long-term stability of 67% S_{br}-MoS_x as the best active catalyst was evaluated through the measurement of linear sweep voltammetry before and after 500 and 1000 cycles. As shown in Fig. 2f, only a negligible potential shift was observed due to the formation of H_2 bubbles on the electrode [21]. Hence, we believed that the S_{br}-MoS_x has the potential to become a highly active electrocatalyst that is sufficiently stable for HER.

3.3. Proposed formation mechanism of S_{br}–MoS_x

The origin of the increased S/Mo ratio and the enhanced bridging S configuration in MoS_x were systematically investigated through various spectroscopy and precipitimetry analyses. Firstly, the interaction between $(NH_4)_2MoS_4$ and $(NH_4)_2S_x$ in the mixture during pre-reaction was analyzed using Raman spectroscopy. As shown in Fig. 3a, the spectra of $(NH_4)_2MoS_4$ displayed two distinct bands at 452 and 485 cm^{-1}, corresponding to the symmetric and antisymmetric Mo–S stretching of MoS_4^{2-} anions, respectively, and the peaks of $(NH_4)_2S_x$ centered at 437 and 470 cm^{-1} were attributed to E_3 and A_1 vibration [30,31]. There are no changes in the structure of $(NH_4)_2MoS_4$ or $(NH_4)_2S_x$ individually aged for 12 h compared to each of the pristine materials. On the other hand, two kinds of broad bands were observed in the mixture of $(NH_4)_2MoS_4$ and $(NH_4)_2S_x$. A broad band in a high wavenumber from 500 to 600 cm^{-1} was attributed to the overlapped band of S—S vibrations of the bridge and terminal S, while the other band from 250 to 400 cm^{-1} was attributed to the overlapped band of Mo-S vibrations of the bridge and terminal S. Interestingly, after aging of the mixture, symmetric and antisymmetric Mo-S vibration peaks of the MoS_4^{2-} anion disappeared, and the broad band corresponding to the vibrations of Mo═S bonds was newly observed. Detailed information on the mixture of $(NH_4)_2MoS_4$ and $(NH_4)_2S_x$ before and after the aging process was obtained from UV–vis spectroscopy. $(NH_4)_2MoS_4$ showed two distinct absorption peaks at 317 and 468 nm that did not change after aging as shown in Fig. 3b. However, the absorption peaks of $(NH_4)_2S_x$ at wavelengths of 300 and 370 nm suddenly decreased after aging due to oxidation and precipitation of S as shown in Fig. 3c. In the case of the mixture of $(NH_4)_2MoS_4$ and $(NH_4)_2S_x$, two absorption peaks related to the $(NH_4)_2MoS_4$ at wavelengths of 310 and 468 nm, and a new absorption peak at 392 nm were observed after aging (Fig. 3d). The appearance of this peak was not attributed to $(NH_4)_2S_x$, but to the formation of molybdenum polysulfide anions such as MoS_9^{2-}, $Mo_2S_{12}^{2-}$, and $Mo_2S_9^{2-}$ [32]. Therefore, it could be presumed that the pre-reaction for the aging step occurred between the MoS_4^{2-} anions and the polysulfide anions due to the instability of MoS_4^{2-} anions in the mixture, and this led to the formation of the aforementioned types of molybdenum polysulfide anions. To identify the generated anions, we selectively precipitated the anions by the addition of suitable cations such as ammonium, tetraethylammonium and tetraphenylphosphonium. Molybdenum polysulfide anions, as combined with specific

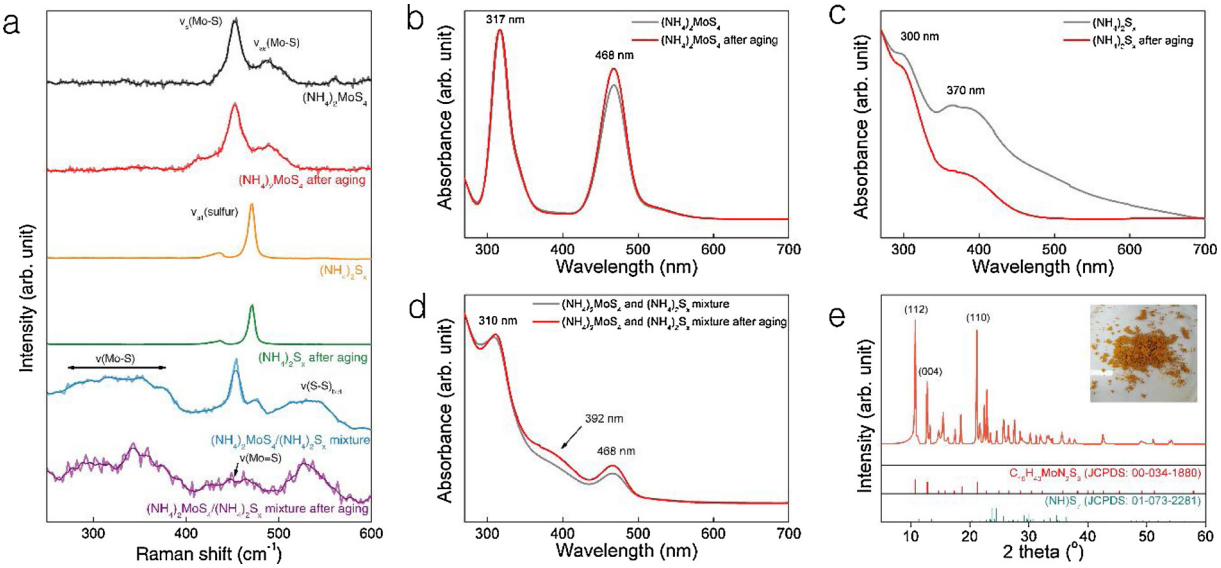

Fig. 3. (a) Raman and (b–d) UV/vis spectra of $(NH_4)_2MoS_4$ solution, $(NH_4)_2S_x$ solution, and their mixture before and after aging for 12 h, (e) XRD diffractogram of powder precipitated using tetraethylammonium chloride.

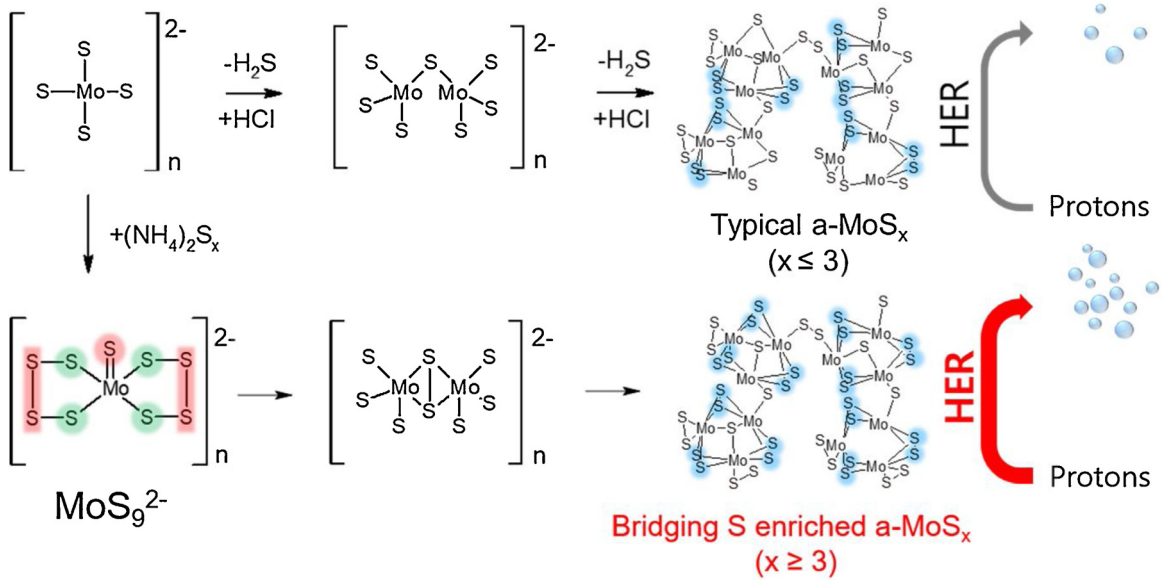

Fig. 4. Schematic of the formation mechanism and proposed structure of typical a-MoS_x and S_{br}-MoS_x.

cations such as ammonium, tetraethylammonium and tetraphenylphosphonium, produced typically arranged crystal structures, such as $(NH_4)_2Mo_2S_{12}$, $(Et_4N)_2MoS_9$, and $(PPh_4)_2Mo_2S_9$, respectively [32–34]. When tetraethylammonium cations were added into the $(NH_4)_2MoS_4$ and $(NH_4)_2S_x$ mixture, a yellow–brown powder was obtained (inset of Fig. 3e). As expected, other cations such as ammonium and tetraphenylphosphonium did not react and no solid powder was obtained. Fig. 3e shows the X-ray diffractogram of the yellow–brown product. The strong peaks corresponding to (112), (004) and (110) planes of $(Et_4N)_2MoS_9$ were observed, along with ammonium polysulfide as by-product. Therefore, it is believed that the pre-reaction for aging induced the generation of the main product of MoS_9^{2-} anions in addition to some intermediates containing terminal S, bridging S, and Mo═S such as MoS_7^{2-} and MoS_5^{2-} anions.Based on the spectroscopy and precipitimetry analyses, we proposed the estimated formation mechanism of a-MoS_x and S_{br}-MoS_x from $(NH_4)_2MoS_4$ as a precursor (Fig. 4). In general, a-MoS_x was prepared by following steps. Firstly, S^{2-} ligand of the MoS_4^{2-} anion was oxidized by proton transfer from HCl and simultaneous generation of gaseous H_2S. Subsequently, Mo^{6+} in MoS_4^{2-} was reduced to Mo^{4+} by the process of electron transfer, leading to formation of $Mo_2S_7^{2-}$ intermediate [30,35]. Thereafter, randomly bonded a-MoS_x particles, composed of Mo_xS_y clusters (where the average ratio of S/Mo is 3), were formed due to the continuous oxidation of S^{2-} ligands in the MoS_4^{2-} anions [32]. On the other hand, in case of S_{br}-MoS_x, MoS_4^{2-} was reacted with $(NH_4)_2S_x$ before oxidation as pre-reaction. This included the continuous exchange of S between MoS_4^{2-} anions and $(NH_4)_2S_x$, resulting in the generation of molybdenum polysulfide anions (mainly MoS_9^{2-}). It was presumed that oxidation state of Mo in MoS_9^{2-} was mainly +4 (Fig. S5) because Mo^{6+} in MoS_4^{2-} was reduced to Mo^{4+} after S exchange due to the generation of polysulfides in MoS_9^{2-} [32]. The resulting MoS_9^{2-} contained various S configurations such as bridging S_2^{2-}, terminal S^{2-}, and Mo═S. Among those S configurations, some parts of the terminal S^{2-} in polysulfide and Mo═S (reddish area in Fig. 4) was preferentially oxidized to H_2S gas by treatment with HCl, and then the remaining S-species (greenish area in Fig. 4) were covalently bonded with adjacent

oxidized MoS_x anions, and they finally transitioned to bridging S_2^{2-} during the oxidation. Ultimately, the higher S/Mo ratio in MoS_9^{2-} as compared to that in MoS_4^{2-} facilitates the formation of the bridging S_2^{2-} configuration during oxidation, thus leading to the generation of bridging S enriched MoS_x with the high S/Mo ratio. Since the bridging S act as the major active site for HER, the S_{br}-MoS_x exhibited enhanced electrochemical HER activity due to a higher proportion of bridging S (bluish area in Fig. 4).

4. Conclusions

The degree of bridging S configuration in amorphous MoS_x was easily controlled by pre-reaction for aging between ammonium tetrathiomolybdate and ammonium polysulfide as a precursor and an additional S source, respectively. The S/Mo ratio and atomic percent of bridging S to the entire S content of MoS_x increased up to 3.5 and 67%, respectively, even though the same for common a-MoS_x were only 2.8 and 47%, respectively. 67% S_{br}-MoS_x shows excellent HER activity with low onset potential (-96 mV) and Tafel slope (46 mV dec^{-1}). This is due to the increase in bridging S configuration caused by the chemical reaction between $(NH_4)_2MoS_4$ and $(NH_4)_2S_x$, leading to the generation of MoS_9^{2-}. The newly designed methodology to enhance the S/Mo ratio in MoS_9^{2-} could be facilitated by promoting the formation of bridging S configuration since bridging S sites are the most active for HER.

Declaration of Competing Interest

The authors declare that they have no known competing financial interests or personal relationships that could have appeared to influence the work reported in this paper.

Acknowledgements

This work was supported by a grant from the National Research Foundation of Korea (NRF) (NRF-2018R1D1A1B07045368 and NRF-2018M1A2A2061989), the Korea Institute of Science and Technology (KIST) Institutional program, and the Industrial Core Technology Development Program funded by the Ministry of Trade, Industry and Energy, Republic of Korea (No. 10052760).

Appendix A. Supplementary data

Supplementary material related to this article can be found, in the online version, at doi:https://doi.org/10.1016/j.apcatb.2019.117995.

References

[1] A. Eftekhari, Electrocatalysts for hydrogen evolution reaction, Int. J. Hydrogen Energy 42 (2017) 11053–11077, https://doi.org/10.1016/j.ijhydene.2017.02.125.
[2] M. Zeng, Y. Li, Recent advances in heterogeneous electrocatalysts for the hydrogen evolution reaction, J. Mater. Chem. A Mater. Energy Sustain. 3 (2015) 14942–14962, https://doi.org/10.1039/C5TA02974K.
[3] L.J. Yang, Y.Q. Deng, X.F. Zhang, H. Liu, W.J. Zhou, $MoSe_2$ nanosheet/MoO_2 nanobelt/carbon nanotube membrane as flexible and multifunctional electrodes for full water splitting in acidic electrolyte, Nanoscale 10 (2018) 9268–9275, https://doi.org/10.1039/C8NR01572D.
[4] Z. Xing, Q. Liu, A.M. Asiri, X. Sun, Closely interconnected network of molybdenum phosphide nanoparticles: a highly efficient electrocatalyst for generating hydrogen from water, Adv. Mater. 26 (2014) 5702–5707, https://doi.org/10.1002/adma.201401692.
[5] T.F. Jaramillo, K.P. Jørgensen, J. Bonde, J.H. Nielsen, S. Horch, I. Chorkendorff, Identification of active edge sites for electrochemical H_2 evolution from MoS_2 nanocatalysts, Science 317 (2007) 100–102, https://doi.org/10.1126/science.1141483.
[6] T.-W. Lin, C.-J. Liu, J.-Y. Lin, Facile synthesis of MoS_3/carbon nanotube nanocomposite with high catalytic activity toward hydrogen evolution reaction, Appl. Catal. B 134–135 (2013) 75–82, https://doi.org/10.1016/j.apcatb.2013.01.004.
[7] D. Merki, S. Fierro, H. Vrubel, X. Hu, Amorphous molybdenum sulfide films as catalysts for electrochemical hydrogen production in water, Chem. Sci. 2 (2011) 1262–1267, https://doi.org/10.1039/C1SC00117E.
[8] H. Vrubel, D. Merki, X. Hu, Hydrogen evolution catalyzed by MoS_3 and MoS_2 particles, Energy Environ. Sci. 5 (2012) 6136–6144, https://doi.org/10.1039/C2EE02835B.
[9] Y. Deng, Z. Liu, A. Wang, D. Sun, Y. Chen, L. Yang, J. Pang, H. Li, H. Li, H. Liu, W. Zhou, Oxygen-incorporated MoX (X: S, Se or P) nanosheets via universal and controlled electrochemical anodic activation for enhanced hydrogen evolution activity, Nano Energy 62 (2019) 338–347, https://doi.org/10.1016/j.nanoen.2019.05.036.
[10] R. Li, L. Yang, T. Xiong, Y. Wu, L. Cao, D. Yuan, W. Zhou, Nitrogen doped MoS2 nanosheets synthesized via a low-temperature process as electrocatalysts with enhanced activity for hydrogen evolution reaction, J. Power Sources 356 (2017) 133–139, https://doi.org/10.1016/j.jpowsour.2017.04.060.
[11] L. Zhao, J. Jia, Z. Yang, J. Yu, A. Wang, Y. Sang, W. Zhou, H. Liu, One-step synthesis of CdS nanoparticles/MoS_2 nanosheets heterostructure on porous molybdenum sheet for enhanced photocatalytic H_2 evolution, Appl. Catal. B Environ. 210 (2017), https://doi.org/10.1016/j.apcatb.2017.04.003 290–269.
[12] W. Zhou, J. Jia, J. Lu, L. Yang, D. Hou, G. Li, S. Chen, Recent developments of carbon-based electrocatalysts for hydrogen evolution reaction, Nano Energy 28 (2016) 29–43, https://doi.org/10.1016/j.nanoen.2016.08.027.
[13] L. Yang, W. Zhou, J. Lu, D. Hou, Y. Ke, G. Li, Z. Tang, X. Kang, S. Chen, Hierarchical spheres constructed by defect-rich MoS_2/carbon nanosheets for efficient electrocatalytic hydrogen evolution, Nano Energy 22 (2016) 409–498, https://doi.org/10.1016/j.nanoen.2016.02.056.
[14] Z. Pu, Q. Liu, A.M. Asiri, Y. Luo, X. Sun, Y. He, 3D macroporous MoS_2 thin film: in situ hydrothermal preparation and application as a highly active hydrogen evolution electrocatalyst at all pH values, Electrochim. Acta 168 (2015) 133–138, https://doi.org/10.1016/j.electacta.2015.04.011.
[15] L. Zhang, X. Ji, X. Ren, Y. Ma, X. Shi, Z. Tian, A.M. Asiri, L. Chen, Electrochemical Ammonia synthesis via nitrogen reduction reaction on a MoS2 catalyst: theoretical and experimental studies, Adv. Mater. 30 (2018) 1800191, , https://doi.org/10.1002/adma.201800191.
[16] X. Li, T. Li, Y. Ma, Q. Wei, W. Qiu, H. Guo, X. Shi, P. Zhang, A.M. Asiri, L. Chen, B. Tang, X. Sun, Boosted electrocatalytic N_2 reduction to NH_3 by defect-rich MoS_2 nanoflower, Adv. Energy Mater. 8 (2018) 1801357, , https://doi.org/10.1002/aenm.201801357.
[17] X. Ren, J. Zhao, Q. Wei, Y. Ma, H. Guo, Q. Liu, Y. Wang, G. Cui, A.M. Asiri, B. Li, B. Tang, High-performance N_2-to-NH_3 conversion electrocatalyzed by Mo_2C nanorod, ACS Cent. Sci. 5 (2019) 116–121, https://doi.org/10.1021/acscentsci.8b00734.
[18] D. Kong, H. Wang, J.J. Cha, M. Pasta, K.J. Koski, J. Yao, Y. Cui, Synthesis of MoS_2 and $MoSe_2$ films with vertically aligned layers, Nano Lett. 13 (2013) 1341–1347, https://doi.org/10.1021/nl400258t.
[19] J. Kibsgaard, Z. Chen, B.N. Reinecke, T.F. Jaramillo, Engineering the surface structure of MoS2 to preferentially expose active edge sites for electrocatalysis, Nat. Mater. 11 (2012) 963, https://doi.org/10.1038/nmat3439.
[20] Z. Chen, D. Cummins, B.N. Reinecke, E. Clark, M.K. Sunkara, T.F. Jaramillo, Core–shell MoO_3–MoS_2 nanowires for hydrogen evolution: a functional design for electrocatalytic materials, Nano Lett. 11 (2011) 4168–4175, https://doi.org/10.1021/nl2020476.
[21] Y. Li, H. Wang, L. Xie, Y. Liang, G. Hong, H. Dai, MoS2 nanoparticles grown on graphene: an advanced catalyst for the hydrogen evolution reaction, J. Am. Chem. Soc. 133 (2011) 7296–7299, https://doi.org/10.1021/ja201269b.
[22] Z. Huang, W. Luo, L. Ma, M. Yu, X. Ren, M. He, S. Polen, K. Click, B. Garrett, J. Lu, K. Amine, C. Hadad, W. Chen, A. Asthagiri, Y. Wu, Dimeric $[Mo_2S1_2]^{2-}$ cluster: a molecular analogue of MoS_2 edges for superior hydrogen-evolution electrocatalysis, Angew. Chem. Int. Ed. 54 (2015) 15181–15185, https://doi.org/10.1002/anie.201507529.
[23] J. Kibsgaard, T.F. Jaramillo, F. Besenbacher, Building an appropriate active-site motif into a hydrogen-evolution catalyst with thiomolybdate $[Mo_3S_{13}]^{2-}$ clusters, Nat. Chem. 6 (2014) 248, https://doi.org/10.1038/nchem.1853.
[24] C.-H. Lee, S. Lee, Y.-K. Lee, Y.C. Jung, Y.-I. Ko, D.C. Lee, H.-I. Joh, Understanding the origin of formation and active sites for thiomolybdate $[Mo_3S_{13}]^{2-}$ clusters as hydrogen evolution catalyst through the selective control of sulfur atoms, ACS Catal. 8 (2018) 5221–5227, https://doi.org/10.1021/acscatal.8b01034.
[25] L.R.L. Ting, Y. Deng, L. Ma, Y.-J. Zhang, A.A. Peterson, B.S. Yeo, Catalytic activities of sulfur atoms in amorphous molybdenum sulfide for the electrochemical hydrogen evolution reaction, ACS Catal. 6 (2016) 861–867, https://doi.org/10.1021/acscatal.5b02369.
[26] Z. Ye, J. Yang, B. Li, L. Shi, H. Ji, L. Song, H. Xu, Amorphous molybdenum Sulfide/Carbon nanotubes hybrid nanospheres prepared by ultrasonic spray pyrolysis for electrocatalytic hydrogen evolution, Small 13 (2017) 1700111, , https://doi.org/10.1002/smll.201700111.
[27] T. Wang, J. Zhuo, K. Du, B. Chen, Z. Zhu, Y. Shao, M. Li, Electrochemically fabricated polypyrrole and MoSx copolymer films as a highly active hydrogen evolution electrocatalyst, Adv. Mater. 26 (2014) 3761–3766, https://doi.org/10.1002/adma.201400265.
[28] C.-H. Lee, J.-M. Yun, S. Lee, S.M. Jo, K. Eom, D.C. Lee, H.-I. Joh, T.F. Fuller, Bi-axial grown amorphous MoSx bridged with oxygen on r-GO as a superior stable and efficient nonprecious catalyst for hydrogen evolution, Sci. Rep. 7 (2017) 41190, https://doi.org/10.1038/srep41190.
[29] H.W. Wang, P. Skeldon, G.E. Thompson, XPS studies of MoS_2 formation from ammonium tetrathiomolybdate solutions, Surf. Coat. Technol. 91 (1997) 200–207, https://doi.org/10.1016/S0257-8972(96)03186-6.
[30] T. Weber, J.C. Muijsers, J.W. Niemantsverdriet, Structure of amorphous MoS_3, J. Phys. Chem. 99 (1995) 9194–9200, https://doi.org/10.1021/j100022a037.
[31] A.T. Ward, Raman spectroscopy of sulfur, sulfur-selenium, and sulfur-arsenic

mixtures, J. Phys. Chem. 72 (1968) 4133–4139, https://doi.org/10.1021/j100858a031.
[32] M. Draganjac, E. Simhon, L.T. Chan, M. Kanatzidis, N.C. Baenziger, D. Coucouvanis, Synthesis, interconversions, and structural characterization of the molybdenum sulfide anions, $[(S4)_2Mo_S]^{2-}$, $[(S4)_2MoO]^{2-}$, $(Mo_2S_{10})^{2-}$ and $(Mo_2S_{12})^2$, Inorg. Chem. 21 (1982) 3321–3332, https://doi.org/10.1021/ic00139a014.
[33] A. Müller, W.-O. Nolte, B. Krebs, $[(S2)_2Mo(S_2)_2Mo(S_2)_2]^{2-}$, a novel complex containing only S ligands and a Mo–Mo bond, Angew. Chem. Int. Ed. 17 (1978) 279, https://doi.org/10.1002/anie.197802791.
[34] W.H. Pan, M.A. Harmer, T.R. Halbert, E.I. Stiefel, Induced internal redox processes in molybdenum-sulfur chemistry: conversion of tetrathiomolybdate(2-) ion to octathiodimolybdate(2-) ion by organic disulfides, J. Am. Chem. Soc. 106 (1984) 459–460, https://doi.org/10.1021/ja00314a054.
[35] A. Müller, W. Jaegermann, J.H. Enemark, Disulfur complexes, Coord. Chem. Rev. 46 (1982) 245–280, https://doi.org/10.1016/0010-8545(82)85004-2.